ACS APPLIED MATERIALS & INTERFACES

RESEARCH ARTICLE

www.acsami.org

Self-Organized TiO_2 Nanotube Arrays: Synthesis by Anodization in an Ionic Liquid and Assessment of Photocatalytic Properties

Heberton Wender,*[,†] Adriano F. Feil,[†] Leonardo B. Diaz,[†] Camila S. Ribeiro,[‡] Guilherme J. Machado,[†] Pedro Migowski,[§] Daniel E. Weibel,[‡] Jairton Dupont,[§] and Sérgio R. Teixeira*[,†]

[†]Laboratório de Filmes Finos e Fabricação de Nanoestruturas (L3Fnano), UFRGS, Instituto de Física, Av. Bento Gonçalves, 9500, P.O. Box 15051, 91501-970, Porto Alegre, RS, Brazil

[‡]Laboratório de Fotoquímica e Superfícies (LAFOS), UFRGS, Instituto de Química, Av. Bento Gonçalves, 9500, P.O. Box 15003, 91501-970, Porto Alegre, RS, Brazil

[§]Laboratório de Catálise Molecular (LAMOCA), UFRGS, Instituto de Química, Av. Bento Gonçalves, 9500, P.O. Box 15003, 91501-970, Porto Alegre, RS, Brazil

Supporting Information

ABSTRACT: Self-organized TiO_2 nanotube (NT) arrays were produced by anodization in ethylene glycol (EG) electrolytes containing 1-*n*-butyl-3-methyl-imidazolium tetrafluoroborate ($BMI.BF_4$) ionic liquid and water. The morphology of the as-formed NTs was considerably affected by changing the anodization time, voltage, and water and ionic liquid electrolyte concentrations. In general, a nanoporous layer was formed on the top surface of the TiO_2 NTs, except for anodization at 100 V with 1 vol % of $BMI.BF_4$, where the NT's mouth was revealed. The length and bottom diameter of the NTs as well as the pore diameter of the top layer showed a linear relationship with increased anodization voltage. These TiO_2 NTs were tested as photocatalysts for methyl orange photodegradation and hydrogen evolution from water/methanol solutions by UV light irradiation. The results show that the TiO_2 NTs obtained by anodization in $EG/H_2O/BMI.BF_4$ electrolytes are active and efficient for both applications.

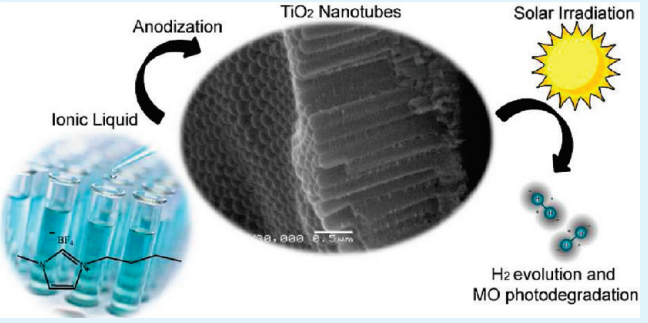

KEYWORDS: TiO_2 nanotubes, ionic liquid electrolytes, water splitting, photocatalysis, hydrogen generation

1. INTRODUCTION

The need for new energy resources, such as solar energy conversion, has evolved in recent decades into the search of innovative photovoltaic materials.[1] One of the most promising forms of clean energy generation and storage is molecular hydrogen. Hydrogen can be used for electricity generation in fuel cells or in combustion engines, with water as the only byproduct. However, finding an environmentally friendly source of hydrogen gas is an important challenge, since the current industrial processes for H_2 generation are still dependent on fossil fuels,[1] generating large amounts of greenhouse gases. In this scenario, the photocatalytic splitting of water into O_2 and H_2 is an interesting alternative. It has been shown that wide band gap materials such as TiO_2 can be used for photocatalytic water splitting under solar radiation.[2] Moreover, due to its relatively low cost and photostability, TiO_2 has been recognized as a promising material for other photochemical applications.[3]

Environmental problems such as water and air pollution have also attracted worldwide attention, and substantial fundamental and applied research on environmental remediation based on TiO_2 applications has been carried out.[2−4] Recently, it has been reported that nanotubular TiO_2 anodes possess better photochemical activity than photoanodes composed of TiO_2 particles.[5,6] Apparently, the large specific surface area of the TiO_2 nanotubes (NTs) results in the enhancement of its photocatalytic activity and, as a consequence, the interest in TiO_2 NT preparation by various methods has increased in recent years. The synthesis of TiO_2 NTs has been carried out using a well-aligned ZnO template nanorod array film and the sol−gel process,[7] hydrothermal treatment,[8] and anodic oxidation.[6,9] In this regard, the anodization process represents a low-cost method to produce highly organized oxide nanomaterials[10−13] for distinct applications.[14]

In the case of anodization of Ti foils or films, it has been shown that the presence of F^- or Cl^- ions in the anodization electrolyte induces formation of TiO_2 NT arrays.[15] An oxidation/dissolution/etching model has been used to explain the formation of this interesting structure.[16] Since TiO_2 is active only in the ultraviolet range,[17,18] new electrolytes have been employed in order to

Received: February 4, 2011
Accepted: March 28, 2011
Published: March 28, 2011

impregnate in TiO_2 NTs with small quantities of atoms, such as P, B, C, or N, thus altering its band gap and increasing the absorption of light in the visible range.[17] Moreover, the controlled use of new electrolytes can propitiate new properties on anodic oxides, such as improved growth rate and geometry control (length, diameter, tube wall thickness, etc.).

The use of imidazolium ionic liquids (IL)[19−21] as a template, electrolyte, or solvent to obtain TiO_2 NTs is quite recent with just a few studies reporting their use.[22,23] The first study on Ti anodization with ionic liquids was reported by Schmuki and co-workers.[22] It was shown that anodization in the ionic liquid (IL) 1-*n*-butyl-3-methyl-imidazolium tetrafluoroborate ($BMI.BF_4$) can be used directly to grow well-defined layers of self-organized TiO_2 NTs on a Ti surface. The resulting nanotube layers had a thickness in the range of approximately 300−650 nm, with individual tubes of diameters between 27 and 43 nm. When anodization was conducted in the water immiscible IL 1-*n*-butyl-3-methyl-imidazolium hexafluorophosphate ($BMI.PF_6$), no NTs were formed. However, Misra and co-workers[23] have shown that when Ti was anodized in an electrolyte composed of an ethylene glycol/water (EG/H_2O) solution with 0.6 vol % of $BMI.BF_4$, the formation of a double-walled TiO_2 NTs structure occurred. The authors showed that, compared to similar single-walled TiO_2 NTs and commercial TiO_2 nanoparticles, these double-walled TiO_2 NTs displayed 2−4 times more photoactivity in terms of hydrogen generation under solar light illumination by the splitting of water. Therefore, due to the interesting properties shown by the incorporation of $BMI.BF_4$ in the anodization electrolyte, it is attractive to extend and characterize the NT formation process in conditions different from those in which it has been previously reported.[23] Also, the study TiO_2 NT photocatalytic activity is of great importance for successful applications.

This study reports on the synthesis of self-organized single-walled TiO_2 NT arrays by anodization in electrolytes composed of ethylene glycol (EG), water, and $BMI.BF_4$. Herein, we investigated the effects of the various parameters that control TiO_2 NT arrays growth, such as anodization time, applied voltage, water, and $BMI.BF_4$ concentrations in the electrolyte. Additionally, the photocatalytic activity of the prepared TiO_2 NT arrays was tested for the methyl orange (MO) photodegradation, a typical stable and difficult to degrade azo dye, and for photocatalytic hydrogen generation through water splitting.

2. EXPERIMENTAL SECTION

2.1. General Considerations. Methyl orange (MO), ethylene glycol (EG, 99.8%) and titanium foils (Ti, 0.25 mm thick, 99.6%) were purchased from Sigma-Aldrich, Synth and Goodfellow, respectively. $BMI.BF_4$ ionic liquid was synthesized as described in previous reports[24,25] and evacuated for 2 h at room temperature prior to anodization.

2.2. TiO_2 NT Preparation. TiO_2 NT arrays were prepared by anodization of 1 cm diameter Ti sheets in electrolytes composed of EG, distilled water (from 0 to 30 vol %), and $BMI.BF_4$ IL (from 0.6 to 1.5 vol %). Prior to each anodization, Ti samples were cleaned with acetone followed by a distilled water rinse. Anodization was performed at room temperature using a standard two-electrode cell,[23,26] with Ti foil as the anode and platinum foil (3 cm diameter) as the cathode under constant applied voltage in the 20−100 V range. The distance between the electrodes was maintained at 3 cm in all experiments. After the anodization process, all the samples were rinsed with distilled water and dried in air at room temperature.

2.3. TiO_2 NT Characterization. The TiO_2 NTs morphology was characterized by scanning electron microscopy (SEM) using JEOL 6060 equipment. High resolution glancing-incident angle X-ray diffraction (GI-XRD) was carried out at the Brazilian Synchrotron Light Laboratory (LNLS) at the D10A-XRD2 beamline. In situ heating of the samples was investigated to study the dependence of the sample crystallinity with temperature. As a first step, each sample was heated directly to 400 °C with a heating rate of 20 $°C \cdot min^{-1}$. Then, without cooling, new measurements were carried out at 500 and 600 °C.

2.4. Photocatalytic Activity Measurements. MO water solutions (35 mL) with concentrations of 10 ppm were prepared to evaluate the photocatalytic activity of the anatase phase of TiO_2 NTs annealed at 400 °C for 3 h. TiO_2 NTs were set in a specially built Teflon support in the center of a photochemical reactor made of quartz. Photocatalysis of MO solutions were carried out at room temperature with continuous stirring by a magnetic Teflon bar. UV and visible light irradiation were obtained from a 150 W mercury−xenon lamp (Sciencetech Inc.) operating at about 78% power. The light beam was focused to homogeneously cover the entire photocatalyst surface (1.23 cm^2). The photocatalytic activity was evaluated as the percentage disappearance of the dye based on the decrease of the absorbance band of MO at 464 nm recorded at regular time intervals following UV illumination. The residual MO was measured, and thus, the percentage of MO degradation was obtained. A UV-1601PC-VIS spectrophotometer (Shimadzu Co. Japan) was used to measure the change in MO absorbance.

Experiments on the photogeneration of hydrogen by water splitting were carried out in a calibrated gas-closed photochemical reactor made of Teflon as previously described.[11] Prior to irradiation, the system was deaerated by bubbling argon through the reactor using custom-made Teflon valves. Photocatalytic activities of the TiO_2 NTs were evaluated by measuring hydrogen production by gas chromatography at room temperature typically from a 20 vol % methanol/water solution. Analyses were conducted on an Agilent 6820 GC Chromatograph equipped with a thermal conductivity detector (TCD) and a 5 Å molecular sieve packed column with argon as the carrier gas. Using a gastight syringe with a maximum volume of 500 μL, the amount of hydrogen produced was measured in 1 h intervals.

3. RESULTS AND DISCUSSION

3.1. Investigation of Nanotube Growth. In order to investigate and optimize nanotubes growth in $BMI.BF_4$ IL dissolved in an ethylene glycol electrolyte, Ti anodization was carried out by separately controlling the anodization time, voltage, water content, and $BMI.BF_4$ concentration. To investigate time and voltage, the anodizations were performed in a fixed EG/H_2O mixture (100:10 v/v) with 0.6 vol % $BMI.BF_4$ ensuring that the electrolyte properties, such as conductivity and viscosity, were all the same. SEM images of TiO_2 NTs obtained with different times of anodization at an applied voltage of 60 V can be seen in Figure S1 in the Supporting Information. The TiO_2 NT length and bottom diameter as a function of anodization time are summarized in Figure 1a,b, respectively. It was noted that a porous layer formed on the top surface of the NTs in all conditions; therefore, we chose to measure the bottom diameter as well as the pore diameter of the TiO_2 NTs and not the NT's mouth diameter. Hereafter, surface diameter (Figure 1b) will refer to the pore diameter of the top layer above the NTs. In the first minute of anodization, only a thin nanoporous titanium dioxide layer was formed (Figure S1, Supporting Information) and after 5 min, nanotubular geometry started to be formed. Further anodization increased the length and bottom diameter NTs, up to 30 min.

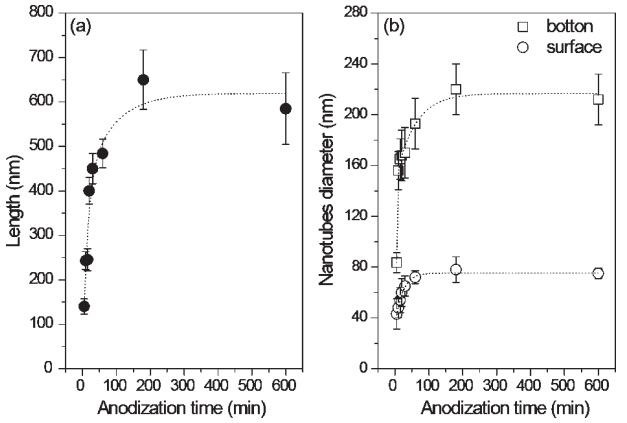

Figure 1. Summary of TiO_2 NTs length (a) and bottom and surface pore diameters (b) after anodization in EG/water (100:10 v/v) with 0.6 vol % $BMI.BF_4$ at 60 V as a function of the anodization time.

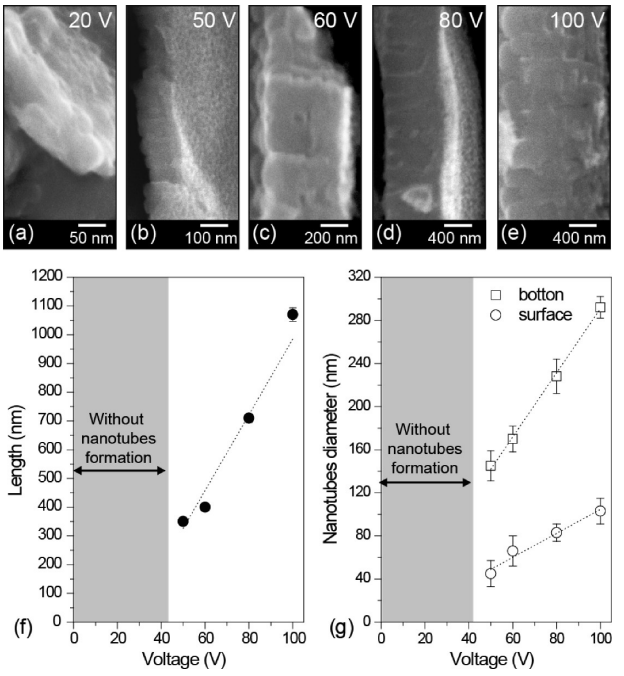

Figure 2. Representative SEM images of TiO_2 NTs (a–e), length (f) and bottom and surface pore diameters (g) after anodization in EG/water (100:10 v/v) with 0.6 vol % $BMI.BF_4$ for 20 min as a function of the applied potential.

From 30 to 180 min of anodization, the NTs continued to grow, however, with a reduced growth rate. Interestingly, the limit of 400 nm for NTs length as reported in a previous study[23] was extended to 640 nm in our experiments. NTs length and bottom diameter both stabilized near 600 and 210 nm, respectively, with further anodization time. The behavior of surface pore diameter was shown to be similar to the NTs bottom diameter.

The effect of the electric field on the TiO_2 NTs formation was investigated by varying the applied potential from 20 to 110 V for 20 min. Figure 2a–e shows SEM images of the TiO_2 NTs anodized at different applied potentials. The corresponding tube length and bottom diameter are summarized in Figure 2f,g, respectively. At 20 V, only a dissolute oxide layer with microholes at the top surface could be observed without any nanotubes

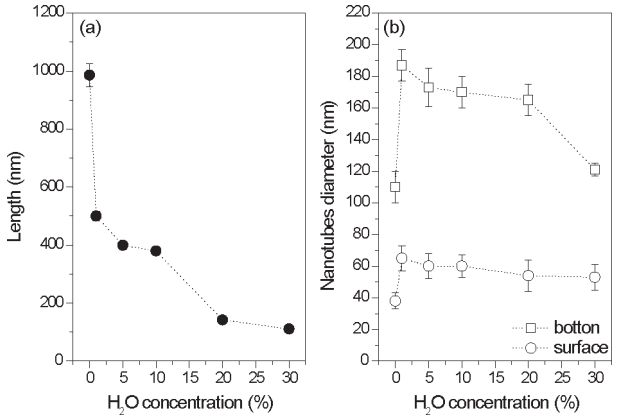

Figure 3. TiO_2 NTs length (a) and bottom and surface pore diameters (b) after 20 min of anodization at 60 V in 0.6 vol % of $BMI.BF_4$ as a function of water content in the electrolyte.

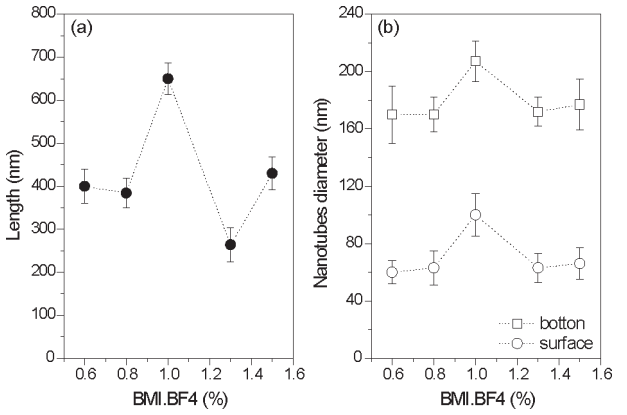

Figure 4. TiO_2 NTs length (a) and bottom and surface pore diameters (b) as a function of $BMI.BF_4$ volume concentration after anodization at 60 V for 20 min.

(Figure 2a). Analyzing Figure 2, it is possible to infer that TiO_2 NTs lengths and bottom diameters, as well as surface layer pore diameters, increased as the applied potential increases, in agreement with previously reported results.[16] When the applied potential increased, the NTs length and diameter increased proportionally, reaching 1070 nm in length and 290 nm as the bottom diameter at 100 V. It is well-known that there are three key processes during the growth of nanotube arrays, i.e., field-assisted oxidation at the metal/oxide interface, field-assisted dissolution at the oxide/electrolyte interface at the tube bottom, and chemical dissolution of produced nanotubes at the tube mouth.[27,28] These processes are responsible for two crucial rates which in turn determine the final length of nanotube arrays: (i) electrochemical etching rate, which is determined by field-assisted oxidation and dissolution and (ii) the chemical dissolution rate, i.e., the rate at which the TiO_2 nanotube arrays is dissolved.[16] As a consequence, longer NTs can be achieved for a given time duration if the electrochemical etching rate at the tube bottom is faster than the chemical dissolution rate at the tube mouth; otherwise, shorter NTs or even no NTs are obtained. In all studied conditions, from 50 to 100 V, the electrochemical etching rate at the TiO_2 NTs bottom was faster than the chemical dissolution rate at the tube mouth.

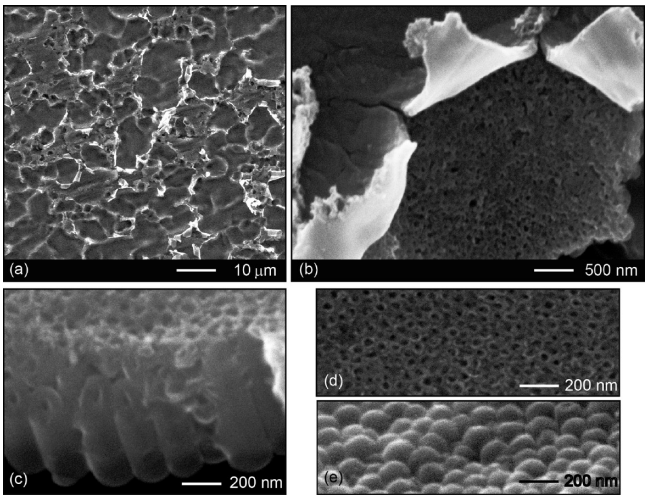

Figure 5. TiO_2 NTs after anodization in EG/water/BMI.BF_4 electrolytes. (a) Micrometric cavities on the top surface of samples. (b) Zoom-scaled image showing the external compact layer and the nanoporous layer inside the cavities. (c) Cross-section SEM image of the vertically aligned TiO_2 NTs with the porous layer at the surface. (d) SEM image of the nanopores at the top of the vertically aligned NTs. (e) SEM image of the smooth NTs bottoms.

Water concentration in the electrolyte was investigated by anodization at 60 V for 20 min (arbitrarily chosen). As can be seen in Figure 3, water concentration was a key factor determining NTs morphology during anodization in the EG/BMI.BF_4 electrolyte. With the increase in water content from 0 to 30 vol %, the length of TiO_2 NTs decreased from 1000 to 100 nm. Bottom diameters increased suddenly to 190 nm with increasing water content from 0 to 1 vol % and then decreased slowly to 120 nm at 30 vol % H_2O. The diameter of the pores on the surface layer followed the same behavior of the NTs bottom diameter as water content increased. Similar trends were found during anodization in pure BMI.BF_4[22] and in a fluoride/glycerol electrolyte.[29] Representative SEM images of TiO_2 NTs after anodization in electrolytes containing from 0 to 30 vol % water are shown in Figure S2 in the Supporting Information.

The effect of ionic liquid concentration in the electrolyte was also investigated by anodizing at 60 V for 20 min and fixing the ratio of EG/H_2O at 100:10 v/v. Figure 4 presents the dependence of TiO_2 NTs length and bottom diameter, as well as surface pore diameter, on the BMI.BF_4 volume content. TiO_2 NTs of approximately 650 nm in length, 208 nm bottom diameter, and 100 nm surface pore diameter were obtained when the BMI.BF_4 volume concentration was 1.0% (see Figure 4). Below and above 1.0 vol %, shorter lengths and smaller diameters were obtained. Typical SEM images of the as-prepared TiO_2 NTs in the concentration interval investigated (from 0.6 to 1.5 vol % BMI.BF_4) are presented in Figure S3 in the Supporting Information. Similar trends were observed when anodization was conducted in acid and organic electrolytes associated with HF or NH_4F.[30]

Under all the above-mentioned anodization conditions, the TiO_2 surface always showed micrometric cavities on its surface (see Figure 5a to better visualize). Inside the cavities (Figure 5b), vertically aligned TiO_2 NTs with a layer of nanopores covering the surface were observed (Figure 5c). The NTs bottoms were smooth, closed, and very well-defined, as were the surface pores (Figure 5d).

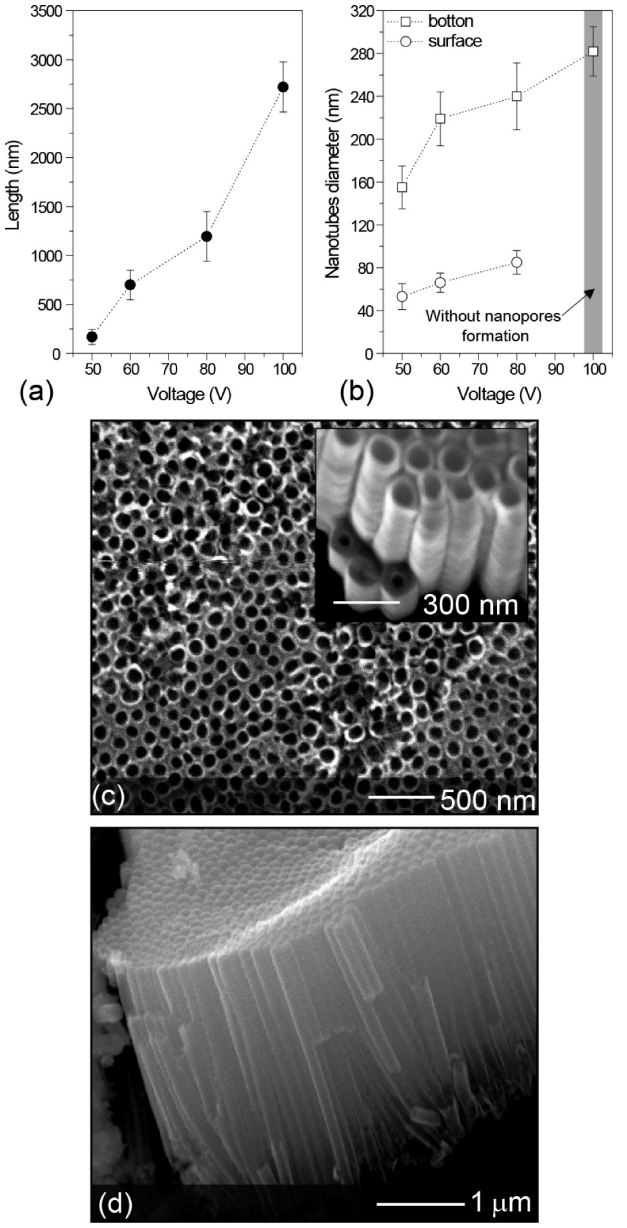

Figure 6. TiO_2 NTs after 20 min of anodization in EG/water (10:100 v/v) + 1.0 vol % BMI.BF_4. (a) NTs length and (b) NTs bottom diameter and surface nanopore diameter as a function of the applied potential. Top-view (c) and cross-section (d) SEM images of TiO_2 NTs anodized at 100 V, showing that the nanopores were removed from of the surface of the NTs.

Recently, Misra and co-workers[23] reported the formation of double-walled TiO_2 NTs using the same system studied here. However, some contrasting results were found: (1) increasing the applied potential from 60 to 80 V did not affect the length of the NTs; (2) NTs did not grow to more than 350 nm under those experimental conditions; (3) NTs were only formed between 60 and 80 V; and (4) anodization with EG/water and BMI.BF_4 IL lead to the formation of double-walled TiO_2 NTs.

Herein, TiO_2 NTs were clearly obtained from 50 to 100 V. When the anodization conditions were varied, the 350 nm limit was exceeded and, in all studied intervals, the NTs length and diameter responded linearly with the applied potential. Double-

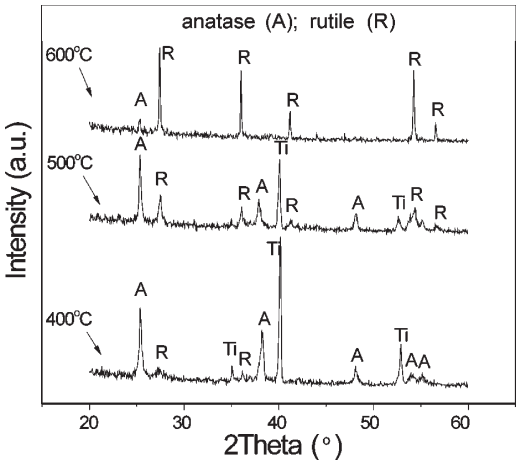

Figure 7. GI-XRD patterns of TiO_2 NTs after anodization in a BMI.BF_4 ionic liquid-based electrolyte.

walled TiO_2 NTs were clearly not reproduced (Figure 5c). It is possible that the pore layer at the top surface of the NTs might have given the false impression of double-walled TiO_2 NTs if they were only observed by a top-view SEM image.

Thus, to improve NTs growth rate and morphology and also to try to remove the top nanoporous layer, anodization for 20 min was performed with different applied voltages with 1.0 vol % BMI.BF_4. The results are shown in Figure 6. The NTs length and bottom diameter increased from 400 to 2800 nm and 155 to 270 nm, respectively, as the applied potential increased from 50 to 100 V. The porous layer continued to cover the top of the NTs in the samples anodized from 50 to 80 V, and the diameter of the pores increased as the applied potential increased. Interestingly, this top layer was removed when anodization was conducted at 100 V, under which conditions the NTs revealed well-defined bottoms, walls, and mouths (Figure 6c,d), similar to the anodization behavior of TiO_2 NTs produced in a conventional fluorine medium.[28]

3.2. Structural Analysis. Figure 7 shows the high resolution GI-XRD patterns of a typical sample obtained by anodization in a BMI.BF_4 IL-based electrolyte, after annealing at 400, 500, and 600 °C in an air atmosphere. The as-fabricated NTs were amorphous, showing only Ti peaks (results not shown). The sample annealed at 400 °C showed a predominantly anatase phase with little evidence of the rutile phase crystallization. When the temperature was increased to 500 °C, a mixture of anatase and rutile phases was obtained. At 600 °C, practically all the TiO_2 was crystallized in the rutile phase.

3.3. Photocatalytic Activity of TiO_2 NTs: Degradation of MO Dye Solutions and Hydrogen Photogeneration by Water Splitting. The photocatalytic activity of the TiO_2 NTs was investigated using only NTs crystallized in the anatase phase (400 °C for 3 h), because this is the most active phase of titania under UV light illumination.[11,31] Figure 8 shows the decolorization results of 10 ppm MO solutions in the presence or absence of TiO_2 NT arrays for different time intervals during darkness adsorption and illumination conditions. It can be seen that no decolorization of MO was observed within 150 min in the presence of the NTs without illumination or after irradiation of the MO solutions in the absence of the NT arrays. These results showed the well-known stability and resistance to degradation of MO solutions. When illumination was carried out in the presence

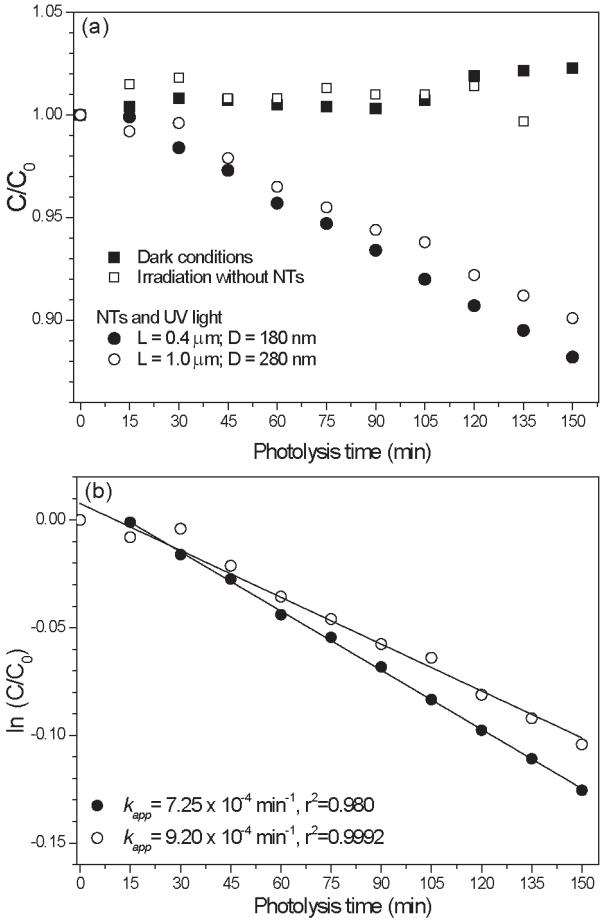

Figure 8. (a) Residual MO at different irradiation times for dark conditions with NTs (filled squares), UV irradiation without TiO_2 NTs (open squares), and irradiated solutions in the presence of NTs of different length (L) and diameter (D) (filled and open circles). (b) Apparent first-order linear plot of $\ln(C_0/C)$ versus the irradiation time of MO degradation kinetics for TiO_2 NT arrays. Filled circles: L = 0.4 μm, D = 180 nm. Open circles: L = 1 μm, D = 280 nm.

of NTs, the percent of residual MO at different UV light time intervals decayed as a function of irradiation time (see Figure 8a). It can also be seen in Figure 8 that changes in the length and diameter of the NTs did not significantly modify the degradation rate.

The rate of the heterogeneous photocatalytic degradation of a dye has been described by the Langmuir−Hinshelwood mechanism[32] which can be expressed by the following mathematical equation:

$$r = -\frac{dC}{dt} = \frac{kK_{ad}C}{1 + K_{ad}C} \quad (1)$$

where r represents the initial rate of photooxidation, C is the variable concentration at any time t, k is the reaction rate constant, and K_{ad} is the adsorption coefficient of the dye on the photocatalyst. If the concentration of the dye is low enough, pseudofirst-order reaction conditions apply and the product $K_{ad}C$ is very small as compared to 1 in the denominator of eq 1. Integrating eq 1 after this simplification:

$$\ln\frac{C_0}{C} = kK_{ad}C = k_{app}t \quad (2)$$

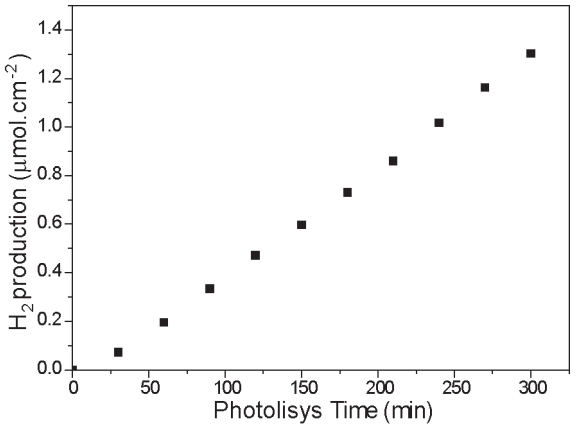

Figure 9. Hydrogen evolution from a 20 vol % methanol/water solution with TiO_2 NTs of 1 μm in length as the photocatalyst under UV illumination.

where $k_{app} = kK_{ad}$ is the apparent pseudofirst-order reaction rate constant and C_0 is the initial concentration of the dye.

Figure 8b shows the linear relationship of the natural logarithm of the ratio between the initial concentration of MO and its concentration after photocatalytic degradation $(\ln(C_0/C))$ versus the corresponding irradiation time. The correlation constants (r^2) for the fitted lines were calculated to be 0.980 and 0.999 (see the legend of Figure 8), which indicates that the photocatalytic degradation of MO can be described by a first-order kinetic model. The value of k_{app} obtained from the slopes of the linear curves shown in Figure 8b gives an indication of the activity of the photocatalyst. The small increase in photodecomposition rate of MO observed with NTs of 1 μm length can be assigned to a higher geometrical surface area of these NTs compared to the shorter ones. No attempt was made to measure the actual surface area of the catalysts.

To further study the photocatalytic properties of the prepared NT arrays, the water splitting reaction by UV irradiation in the presence of the catalysts was investigated. Degradation of organic pollutants (AOP: advance oxidative processes) takes place under aerated conditions with the participation of photogenerated holes. These holes act either directly or indirectly in the degradation process via the generation of hydroxide radicals ($OH^{\bullet}$). Additionally, other effective oxygenating agents such as superoxide ($O_2^{\bullet -}$) or hydroperoxide ($HO_2^{\bullet}$) radicals may be also produced on the surface of TiO_2 by the reduction of atmospheric oxygen.[4,33] These powerful oxidizing agents attack pollutant molecules, ultimately leading to the production of mineralization products. On the other hand, photoinduced production of hydrogen from water takes place under unaerated conditions and is achieved by photogenerated electrons, providing that their energy is sufficient to reduce protons into hydrogen molecules.[33] One of the major disadvantages of semiconductor photocatalytic systems in terms of photoinduced hydrogen production from water is their very low efficiency. That reaction is mainly limited by the recombination reaction between photogenerated electrons and holes.[4,33,34] The recombination rate can be suppressed substantially with the use of electron donors as sacrificial agents. Reactions using sacrificial agents are regarded as half-reactions and are often employed in tests of photocatalytic hydrogen or oxygen evolution. A large variety of sacrificial agents can be used, and their role is to react irreversibly with the photogenerated holes and/or oxygen, increasing the rate of hydrogen production.[33,35−38] Within this group of compounds, alcohols are satisfactory hole scavengers, increasing apparent quantum yields and enhancing rates of photocatalytic hydrogen production.[11] The photogeneration of hydrogen by water splitting was tested using methanol as the sacrificial agent.

Under dark conditions, no formation of hydrogen was detected on both types of TiO_2 NT arrays. On the other hand, when UV light was incident on the NTs, hydrogen production evolved steadily over extended periods of time. Figure 9 shows the amounts of hydrogen evolution at room temperature from a deoxygenated mixture of water with 20 vol % methanol and TiO_2 NTs as the photocatalyst under typical UV irradiation conditions. The rate of hydrogen evolution from TiO_2 NTs with a phase composition of 100% anatase was 0.4 μmol h^{-1} cm^{-2}.

Heterogeneous photocatalysts have many times the potential to be used in water-splitting reactions that produce hydrogen and the degradation of organic pollutants. Recently, numerous contributions have highlighted the relation of the photocatalytic degradation of organic pollutants with simultaneous photogeneration of hydrogen.[39−44] However, the efficiency of both processes is in general different and depends on catalyst properties,[37] particle size,[45] and in particular the kinetics of the chemical reactions that lead to final O_2 and H_2 formation.[46] It is possible to find in the literature a wide variety of publications showing catalytic activities for hydrogen production or degradation of pollutants. To a much lower extent, examples can be found that a particular catalyst can be used efficiently for both processes. The results presented here show that the TiO_2 NT arrays prepared in presence of low $BMI.BF_4$ concentrations have the potential to be used in AOP and hydrogen production reactions over extended periods of time. These processes are carried out at room temperature and represent environmentally friendly methods for wastewater treatment, with simultaneous production of a clean and renewable energy source. The activities of the TiO_2 NTs anodized in $EG/BMI.BF_4$-based electrolytes under visible light illumination are currently being investigated.

4. CONCLUSIONS

TiO_2 NT length and bottom diameter can be controlled by choosing the voltage, water and $BMI.BF_4$ volume content, and anodization time. Increasing the water content reduces the TiO_2 NT growth rate. As expected, a linear increase of NT length and diameter was found when the voltage was increased during anodization from 20 to 100 V. In general, a nanoporous layer was formed at the top surface of the NTs, except when anodization occurred at 100 V with 1 vol % $BMI.BF_4$, under which conditions the NT mouth was revealed. Additionally, a maximum NT growth rate was obtained at 1.0 vol % $BMI.BF_4$. Under the experimental conditions herein reported, highly ordered single-walled TiO_2 NT arrays up to 2.8 μm in length and 280 nm in bottom diameter can be achieved by anodization in $EG/H_2O/BMI.BF_4$ electrolytes over relatively short periods of time (~20 min), in contrast to the recently reported double-walled TiO_2 NTs using $EG/H_2O/BMI.BF_4$ electrolytes. Moreover, the TiO_2 NTs obtained by anodization in $BMI.BF_4$-based electrolytes showed photocatalytic activities for the degradation of pollutants using MO dye as a prototype in AOP and hydrogen generation by the splitting of water in the presence of methanol as the sacrificial agent. The results provided here are highly promising in view of various photocatalytic applications of the prepared

TiO_2 nanotubular anatase catalysts. The photocatalytic activity can even be strongly enhanced if a secondary material, such as a suitable noble metal species, can successfully be deposited into the tubes, thus proving great potential for commercial applications.

■ ASSOCIATED CONTENT

Supporting Information. Figure showing, as a function of the anodization time, the top surface, cross-section, and bottom SEM images of TiO_2 NTs after anodization in EG/water (100:10 v/v) with 0.6 vol % $BMI.BF_4$ at 60 V; figure showing SEM images of TiO_2 NTs after 20 min of anodization at 60 V in 0.6 vol % $BMI.BF_4$ with different EG/water vol % ratios; figure showing, as a function of $BMI.BF_4$ content, SEM images of TiO_2 NTs after 20 min of anodization at 60 V in an electrolyte composed of 10:100 vol % mixture of EG/water. This material is available free of charge via the Internet at http://pubs.acs.org.

■ AUTHOR INFORMATION

Corresponding Author
*E-mail: durao@if.ufrgs.br (S.R.T.); hbtwender@gmail.com (H.W.).

■ ACKNOWLEDGMENT

This work was partially supported by "CNPq, FAPERGS, CAPES, and INCTCatal". Thanks are also due to the "*Centro de Microscopia Eletrônica* (CME) of *Universidade Federal do Rio Grande do Sul*" and the National Synchrotron Light Laboratory (LNLS) for the use of their XRD2 beamline experimental facility.

■ REFERENCES

(1) Grossmann, W. D.; Grossmann, I.; Steininger, K. *Environ. Sci. Technol.* **2010**, *44*, 4849.
(2) Chen, J.; Poon, C.-s. *Build. Environ.* **2009**, *44*, 1899.
(3) Gaya, U. I.; Abdullah, A. H. *J. Photochem. Photobiol. C: Photochem. Rev.* **2008**, *9*, 1.
(4) Fujishima, A.; Zhang, X.; Tryk, D. A. *Surf. Sci. Rep.* **2008**, *63*, 515.
(5) Albu, S. P.; Ghicov, A.; Macak, J. M.; Hahn, R.; Schmuki, P. *Nano Lett.* **2007**, *7*, 1286.
(6) Macak, J. M.; Tsuchiya, H.; Ghicov, A.; Yasuda, K.; Hahn, R.; Bauer, S.; Schmuki, P. *Curr. Opin. Solid State Mater. Sci.* **2007**, *11*, 3.
(7) Qiu, J.; Jin, Z.; Liu, Z.; Liu, X.; Liu, G.; Wu, W.; Zhang, X.; Gao, X. *Thin Solid Films* **2007**, *515*, 2897.
(8) Jitputti, J.; Pavasupree, S.; Suzuki, Y.; Yoshikawa, S. *Jpn. J. Appl. Phys.* **2008**, *47*, 751.
(9) Mor, G. K.; Varghese, O. K.; Paulose, M.; Shankar, K.; Grimes, C. A. *Sol. Energy Mater. Sol. Cells* **2006**, *90*, 2011.
(10) Gong, D.; Grimes, C. A.; Varghese, O. K.; Hu, W. C.; Singh, R. S.; Chen, Z.; Dickey, E. C. *J. Mater. Res.* **2001**, *16*, 3331.
(11) Feil, A. F.; Migowski, P.; Scheffer, F. R.; Pierozan, M. D.; Corsetti, R. R.; Rodrigues, M.; Pezzi, R. P.; Machado, G.; Amaral, L.; Teixeira, S. R.; Weibel, D. E.; Dupont, J. *J. Braz. Chem. Soc.* **2010**, *21*, 1359.
(12) Feil, A. F.; da Costa, M. V.; Amaral, L.; Teixeira, S. R.; Migowski, P.; Dupont, J.; Machado, G.; Peripolli, S. B. *J. Appl. Phys.* **2010**, *107*, 026103.
(13) Feil, A. F.; da Costa, M. V.; Migowski, P.; Dupont, J.; Teixeira, S. R.; Amaral, L. *J. Nanosci. Nanotechnol.* **2011**, *11*, 2330.
(14) Weibel, D. E.; Michels, A. F.; Feil, A. F.; Amaral, L.; Teixeira, S. R.; Horowitz, F. *J. Phys. Chem. C* **2010**, *114*, 13219.
(15) Richter, C.; Panaitescu, E.; Willey, R.; Menon, L. *J. Mater. Res.* **2007**, *22*, 1624.
(16) Sun, L.; Zhang, S.; Sun, X. W.; He, X. *J. Electroanal. Chem.* **2009**, *637*, 6.
(17) Cai, Q. Y.; Paulose, M.; Varghese, O. K.; Grimes, C. A. *J. Mater. Res.* **2005**, *20*, 230.
(18) Yoriya, S.; Grimes, C. A. *Langmuir* **2010**, *26*, 417.
(19) Dupont, J. *J. Braz. Chem. Soc.* **2004**, *15*, 341.
(20) Dupont, J.; Suarez, P. A. Z. *Phys. Chem. Chem. Phys.* **2006**, *8*, 2441.
(21) Migowski, P.; Zanchet, D.; Machado, G.; Gelesky, M. A.; Teixeira, S. R.; Dupont, J. *Phys. Chem. Chem. Phys.* **2010**, *12*, 6826.
(22) Paramasivam, I.; Macak, J. M.; Selvam, T.; Schmuki, P. *Electrochim. Acta* **2008**, *54*, 643.
(23) John, S. E.; Mohapatra, S. K.; Misra, M. *Langmuir* **2009**, *25*, 8240.
(24) Wender, H.; de Oliveira, L. F.; Migowski, P.; Feil, A. F.; Lissner, E.; Prechtl, M. H. G.; Teixeira, S. R.; Dupont, J. *J. Phys. Chem. C* **2010**, *114*, 11764.
(25) Cassol, C. C.; Ebeling, G.; Ferrera, B.; Dupont, J. *Adv. Synth. Catal.* **2006**, *348*, 243.
(26) Allam, N. K.; Grimes, C. A. *Sol. Energy Mater. Sol. Cells* **2008**, *92*, 1468.
(27) Karthik, S.; Mor, G. K.; Prakasam, H. E.; Yoriya, S.; Paulose, M.; Varghese, O. K.; Grimes, C. A. *Nanotechnology* **2007**, *18*, 065707.
(28) Paulose, M.; Shankar, K.; Yoriya, S.; Prakasam, H. E.; Varghese, O. K.; Mor, G. K.; Latempa, T. A.; Fitzgerald, A.; Grimes, C. A. *J. Phys. Chem. B* **2006**, *110*, 16179.
(29) Valota, A.; LeClere, D. J.; Skeldon, P.; Curioni, M.; Hashimoto, T.; Berger, S.; Kunze, J.; Schmuki, P.; Thompson, G. E. *Electrochim. Acta* **2009**, *54*, 4321.
(30) Elsanousi, A.; Zhang, J.; Fadlalla, H.; Zhang, F.; Wang, H.; Ding, X.; Huang, Z.; Tang, C. *J. Mater. Sci.* **2008**, *43*, 7219.
(31) Allam, N. K.; Grimes, C. A. *Langmuir* **2009**, *25*, 7234.
(32) Houas, A.; Lachheb, H.; Ksibi, M.; Elaloui, E.; Guillard, C.; Herrmann, J.-M. *Appl. Catal., B: Environ.* **2001**, *31*, 145.
(33) Ni, M.; Leung, M. K. H.; Leung, D. Y. C.; Sumathy, K. *Renewable Sustainable Energy Rev.* **2007**, *11*, 401.
(34) Fujishima, A.; Zhang, X.; Tryk, D. A. *Int. J. Hydrogen Energy* **2007**, *32*, 2664.
(35) Yang, H.; Yan, J. H.; Lu, Z. G.; Cheng, X.; Tang, Y. G. *J. Alloys Compd.* **2009**, *476*, 715.
(36) Lazarides, T.; McCormick, T.; Du, P. W.; Luo, G. G.; Lindley, B.; Eisenberg, R. *J. Am. Chem. Soc.* **2009**, *131*, 9192.
(37) Maeda, K.; Hashiguchi, H.; Masuda, H.; Abe, R.; Domen, K. *J. Phys. Chem. C* **2008**, *112*, 3447.
(38) Lunawat, P. S.; Senapati, S.; Kumar, R.; Gupta, N. M. *Int. J. Hydrogen Energy* **2007**, *32*, 2784.
(39) Tachikawa, T.; Majima, T. *Langmuir* **2009**, *25*, 7791.
(40) Wu, G. S.; Chen, A. *J. Photochem. Photobiol., A: Chem.* **2008**, *195*, 47.
(41) Patsoura, A.; Kondarides, D. I.; Verykios, X. E. *Catal. Today* **2007**, *124*, 94.
(42) Li, Y. X.; Me, Y. Z.; Peng, S. Q.; Lu, G. X.; Li, S. B. *Chemosphere* **2006**, *63*, 1312.
(43) Kondarides, D. I.; Daskalaki, V. M.; Patsoura, A.; Verykios, X. E. *Catal. Lett.* **2008**, *122*, 26.
(44) Daskalaki, V. M.; Kondarides, D. I. *Catal. Today* **2009**, *144*, 75.
(45) Nishijima, K.; Kamai, T.; Murakami, N.; Tsubota, T.; Ohno, T. *Int. J. Photoenergy* Volume 2008, ID: 173943, DOI: 10.1155/2008/173943.
(46) Tang, J. W.; Durrant, J. R.; Klug, D. R. *J. Am. Chem. Soc.* **2008**, *130*, 13885.